Progress In Electromagnetics Research C, Vol. 109, 153–168, 2021

A Preclinical System for Enhancing the Efficiency of Microwave Breast Cancer Hyperthermia Therapy Using Dielectric Matched Layer and Convex Lenses

Maha R. Abdel-Haleem[1, *], Tamer Abouelnaga[2, 3], Mohammed Abo-Zahhad[1, 4], and Sabah M. Ahmed[4, 5]

Abstract—Convex lenses can be used in adjuvant with microwave sources to produce appropriate focus spots for breast cancer hyperthermia therapy. A preclinical system was assessed using a horn antenna together with a convex lens. The horn antenna was built to accommodate the lens size so as to minimize wave spillover. Here, a modified hyperthermia system was tested on a hemisphere phantom of scattered fibro glandular breast tissue with cancer stages I & II. The focus spots were at different locations and depths (up to 2.7 cm) under the skin layer. Transmission and reflection coefficients at the air-breast phantom interface were calculated to determine the best operating frequency (2.45 GHz) for efficient power absorption. Based on these computations, an external dielectric matched layer was added onto the skin of the breast phantom to decrease reflection that would occur between water and skin. This arrangement increased wave transmission inside the breast without increasing applicator input feed. The system could heat regions of tumor at various locations independently using only one applicator. The whole system was fabricated, and measurements were taken to validate the simulated and analytical results.

1. INTRODUCTION

Thermal therapies, especially hyperthermia therapies, have increasingly been the focus of laboratory and clinical research in cancer treatment. In hyperthermia therapy, thermal sources are either externally or internally delivered to tumors, depending on the method used for conducting the process. The most common hyperthermia treatments use external devices where the energy is non-invasively transmitted to human tissue using electromagnetic (EM) technologies [1–5]. The elevated temperature of a human organ (typically between 40°C and 45°C) causes direct cytotoxicity or increases the sensitivity of the cancerous cells to other therapies such as radiation therapy or chemotherapy [6, 7]. One of the persisting challenges in noninvasive hyperthermia treatment is in focusing EM power to the cancerous tissue while avoiding auxiliary foci in healthy tissue. Another problem is the heterogeneity in breast tissue types (fatty, scattered fibro glandular, heterogeneous dense, and extremely dense) [8] and breast cancer stages (stages I, II, III, and IV) [9]. In all noninvasive microwave hyperthermia, the propagation of EM waves is directed toward or outward the human body. In such scenarios, a propagated wave comprises two paths, with one segment inside the human body and the other in the free-space. Because of the considerable difference in impedances between human tissues and air, the power transmission of the EM wave can

Received 14 October 2020, Accepted 26 January 2021, Scheduled 3 February 2021
* Corresponding author: Maha Raof Abdel-Haleem (maha.raof@ejust.edu.eg).
[1] Department of Electronics and Communications Engineering, Egypt-Japan University of Science and Technology, Alexandria 21934, Egypt. [2] Department of Microstrip Circuits, Electronics Research Institute, Giza, Cairo 12622, Egypt. [3] Department of Electronics and Communication Engineering, Higher Institute of Engineering and Technology, Kafrelsheikh, Egypt. [4] Department of Electronics and Electrical Engineering, Faculty of Engineering, Assiut University, Assiut, Egypt. [5] Department of Mechatronics and Robotics Engineering, E-JUST-Alexandria 21934, Egypt.

be rather inefficient. To improve the EM wave coupling to/from the body, a dielectric material layer with compatible permittivity can be applied on the patient's skin, corresponding to the position of the diseased tissue. This dielectric material is referred to as a dielectric matched layer.

Many researchers have developed thermal therapy systems capable of localized hyperthermia using different kinds of phased array antennas [10–14]. Very high input power is applied to breast tissue to reach the target temperature at the tumor location (above 42°C), as reported in [10]. Previously, only stage I cancer can be treated using thermal therapy [11]. Metamaterial lens applicator has also been intensively studied for breast cancer hyperthermia [15–18]. The concept of adjusting focusing point inside biological tissue depends on the distance between wave source and LHM lens. In [15], a flat left-handed metamaterial (LHM) slab lens is used to form a focus flexible applicator in a heterogeneous breast model. In order to acquire better focusing resolution, more LHM lens applicators need to be added around the diseased breast. In [16], a conformal hyperthermia cylindrical LHM lens using joint heating of multiple sources has been developed to be more maneuverable for tumors located in tissues with curved surface. However, this technique still requires many wave sources to produce a focusing region.

With these drawbacks and challenges in mind, a prototype system for breast cancer hyperthermia therapy was developed. The proposed system was aimed at treating breast cancer of stages I and II in scattered fibro glandular tissue of the breast. In this system, a horn antenna at 2.45 GHz was used to focus EM waves at the tumor region, aided only by a dielectric matched layer on the breast phantom skin and a convex lens as shown in Fig. 1. The selection of an appropriate matched layer material was based on a new reflection and transmission coefficient expression at the breast phantom-air interface.

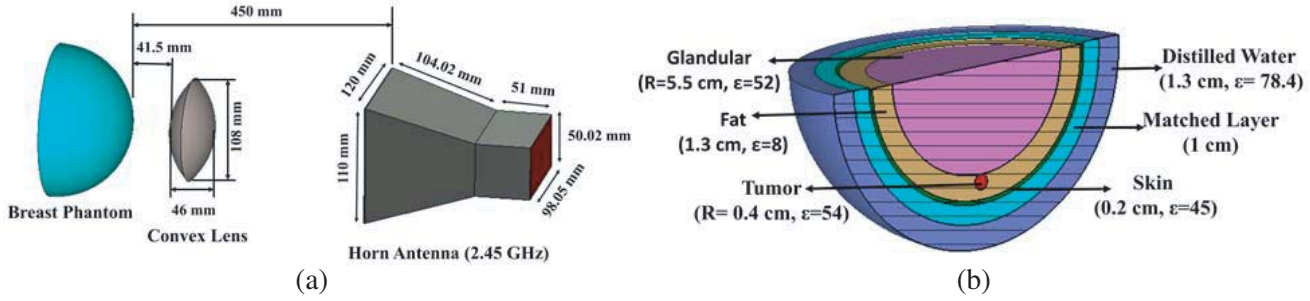

Figure 1. Proposed system. (a) General view. (b) Detailed view of the hemispherical breast phantom with radius ($r = 7$ cm) excluding cooling water and dielectric matched layers.

The paper is organized as follows. In Section 2, a description is given of the prototype system operating frequency and the permittivity of the dielectric matched layer chosen through an analysis of wave transmission and reflection coefficients at the air-breast phantom interface. Simulation scenarios and results of the proposed system are introduced in Section 3. In Section 4, we present a discussion on the simulation concept validation through measurements. The conclusion follows in Section 5.

2. HYPERTHERMIA THERAPY SYSTEM SET UP

The setup of the proposed microwave thermal therapy system was completed over several stages. Firstly, the analyzed EM wave transmission and reflection coefficients at the air-phantom interface were determined at dominant mode for the selection of an appropriate operating frequency for the hyperthermia system. The permittivity of a dielectric matched layer was then determined through proposed formulas. At this point, the obtained optimum frequency is used to build up the antenna. After that, the whole proposed system considering antenna, convex lens, and breast phantom with dielectric matched layer is simulated using multi-physics Computer Simulation Technology (CST) Microwave Studio simulator.

2.1. Transmission and Reflection Coefficient Expressions

In microwave hyperthermia therapy systems, the power directed at the tumor region is transferred from the microwave source through free space to the skin of the breast before penetrating its different layers. This difference in the propagation environment produces a wave impedance mismatch. In the proposed system, wave impedances are classified as being outside or inside the breast phantom. The patient's breast (inside region) can be considered as a spherical dielectric resonator with effective permittivity (ε_{eff}) of breast layers (skin, fat, and glandular tissue) of radius (a). An infinite, linear, homogeneous and isotropic free space represents the outside region. The EM waves can be classified as Transverse Electric (TE) modes and Transverse Magnetic (TM) modes. Spherical electric and magnetic wave equations for the TE modes have been established for the two regions [15]. TE modes inside and outside the breast have different spherical wave impedances. For the outside region (free space, $r > a$), wave impedance comes from electric and magnetic fields in the free space as in Eqs. (1) and (2) [19]

$$Z_{TE(out)} = \frac{E_\theta}{H_\varphi} = -j\eta_0 \frac{\hat{H}_n^{(2)}(k_0 r)}{\hat{H}_n^{(2)'}(k_0 r)} \tag{1}$$

$$\hat{H}_n^{(2)}(k_0 r) = \sqrt{\frac{\pi k_0 r}{2}} H_{n+\frac{1}{2}}^{(2)}(k_0 r) \tag{2}$$

where η_0, k_0, r, $\hat{H}_n^{(2)}(k_0 r)$, $\hat{H}_n^{(2)'}(k_0 r)$, $H_{n+1/2}^{(2)}(k_0 r)$, and $n = 0, 1, 2, \ldots$ are free space wave impedance, wave number, radius of breast phantom, an alternative spherical Hankel function and its derivate, Hankel function of second kind, and order of Hankel functions, respectively.

Figure 2(a) illustrates the behavior of the wave impedance Z_{TE} by plotting X/R, where $Z_{TE} = R + jX$ for the first five modes. Wave impedance is always reactive when $k_0 r < n$ and always resistive when $k_0 r > n$ [19]. For the internal region (effective dielectric of the phantom layers ε_{eff}, $r < a$), wave impedance behavior would change according to the difference of propagation environment. From electromagnetic wave components inside the breast, wave impedance would behave as a standing wave inside a spherical resonator as in Eqs. (3) and (4) [19].

$$Z_{TE(In)} = \frac{E_\theta}{H_\varphi} = \frac{-j\omega\mu_0 \hat{J}_n(kr)}{k\hat{J}_n{}'(kr)} = -j\eta \frac{\hat{J}_n(kr)}{\hat{J}_n{}'(kr)} \tag{3}$$

$$\vec{J_n}(kr) = \sqrt{\frac{\pi kr}{2}} J_{n+\frac{1}{2}}(kr) \tag{4}$$

where η, k, ω, μ_0, $\hat{J}_n(kr)$, $\hat{J}_n'(kr)$, and $J_{n+1/2}(kr)$ are the wave impedance and wave number inside breast phantom, respectively, angular frequency, permeability constant in free space, an alternative spherical Bessel function and its derivate, and Bessel function, respectively.

Figure 2(b) demonstrates the wave impedance behavior inside the resonator for the first five modes. Transmission and reflection coefficients of electromagnetic waves for the TE dominant mode at the breast phantom-air interface can be deduced from wave impedances inside and outside the breast through Eqs. (5) and (6).

$$\Gamma = \frac{\eta - \eta_0}{\eta + \eta_0} = \frac{-\hat{J}_n(kr)\hat{H}_n{}'(k_0 r) + \sqrt{\varepsilon_{eff}}\hat{J}_n{}'(kr)\hat{H}_n(k_0 r)}{-\hat{J}_n(kr)\hat{H}_n{}'(k_0 r) - \sqrt{\varepsilon_{eff}}\hat{J}_n{}'(kr)\hat{H}_n(k_0 r)} \tag{5}$$

$$T = \frac{2\eta}{\eta + \eta_0} = \frac{2\hat{J}_n(kr)\hat{H}_n{}'(k_0 r)}{\hat{J}_n(kr)\hat{H}_n{}'(k_0 r) + \sqrt{\varepsilon_{eff}}\hat{J}_n{}'(kr)\hat{H}_n(k_0 r)} \tag{6}$$

where Γ, T, ε_{eff} are the reflection and transmission coefficients of electromagnetic waves, and the total effective permittivity of breast phantom layers, respectively.

A comparison between obtained and Fresnel reflection coefficient expressions at curved interface in [20] is illustrated in Table 1. The differences between the two expressions are calculated at three points with refraction index ($n = 1.5$) and $kr = 50$ for the verification of the proposed expression.

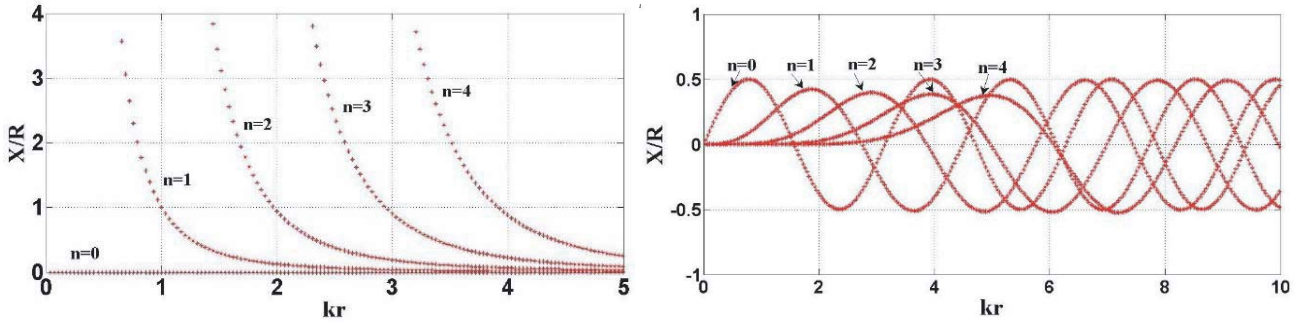

Figure 2. The ratio of wave reactance to resistance for TE dominant mode. (a) Outside breast phantom (free space region). (b) Inside breast phantom (dielectric region with effective permittivity of scattered fibro-glandular breast $\varepsilon = 39$) [21].

Table 1. Comparison between the proposed and Fresnel reflection coefficient formulas.

The Proposed reflection coefficient formula	Fresnel reflection coefficient Formula	Error (%)
0.9152	0.9783	6.4%
0.6602	0.686	3.7%
0.8358	0.8791	5%

2.2. Design of Microwave Applicator

Choosing the optimum frequency that can be utilized for breast cancer hyperthermia therapy is dependent on wave transmission at the air-phantom interface. There is a fundamental trade-off between penetration depth and wave concentration. Lower frequencies produce greater penetration, but there is difficulty in localizing the radiation. On the other hand, wave radiation at higher frequencies renders localization more practicable, but would result in a decrease in penetration depth. Nonetheless, it is easier to design radiators of higher frequencies that fit the body easily.

Transmission and reflection coefficients are calculated for the dominant mode at air-phantom interface as shown in Fig. 3. The distance between the antenna source and air-phantom interface ($d = 45\,\text{cm}$) is only considered in the total system design in simulation. The appropriate operating frequency is chosen to achieve the best transmission, taking cognizance of the trade-off between penetration depth and wave concentration within interesting bandwidth (2–5 GHz). The industrial, scientific, and medical (ISM) radio band comprises a grouping of radio spectra, with the frequencies most exploited being 0.434 GHz, 0.915 GHz, and 2.45 GHz. Many types of microwave radiator are designed for ISM applications [22, 23]. For breast cancer, especially at stages I & II which do not require deep wave penetration, 2.45 GHz was selected for the wave source which produces a maximum transmission coefficient as shown in Fig. 3.

A horn antenna at 2.45 GHz designed for wave application showed very little loss, high gain, and excellent peak power handling capability. The structure was built to accommodate the lens size so as to minimize wave spillover. Even when the antenna is at the exact center of a convex lens, a portion of emitted energy at the edge of the beam will not impinge on the lens which is called beam spillover. There is a trade off between beam spillover and tapered antenna aperture (antenna gain) [24]. The proposed simulated antenna is designed with a spillover efficiency of -1.2 dB calculated using the formulas in [25]. Because of the load effect of the convex lens and breast phantom on antenna, a little shift in antenna reflection coefficient occurs as shown in Fig. 4(a). The antenna introduced a gain of 9.7 dB, sidelobe level of -20.1 dBi, 3 dB beam width of 58°, and 98% efficiency as presented in Figs. 4(b) and (c).

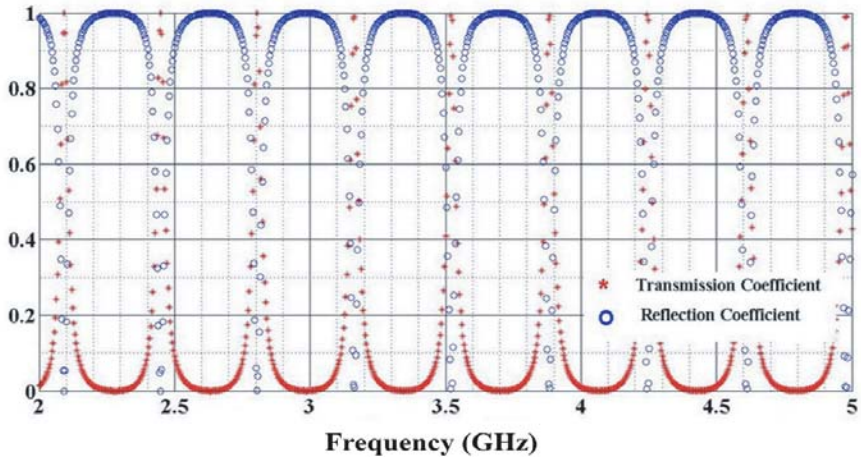

Figure 3. Transmission and reflection coefficients at the phantom-air interface.

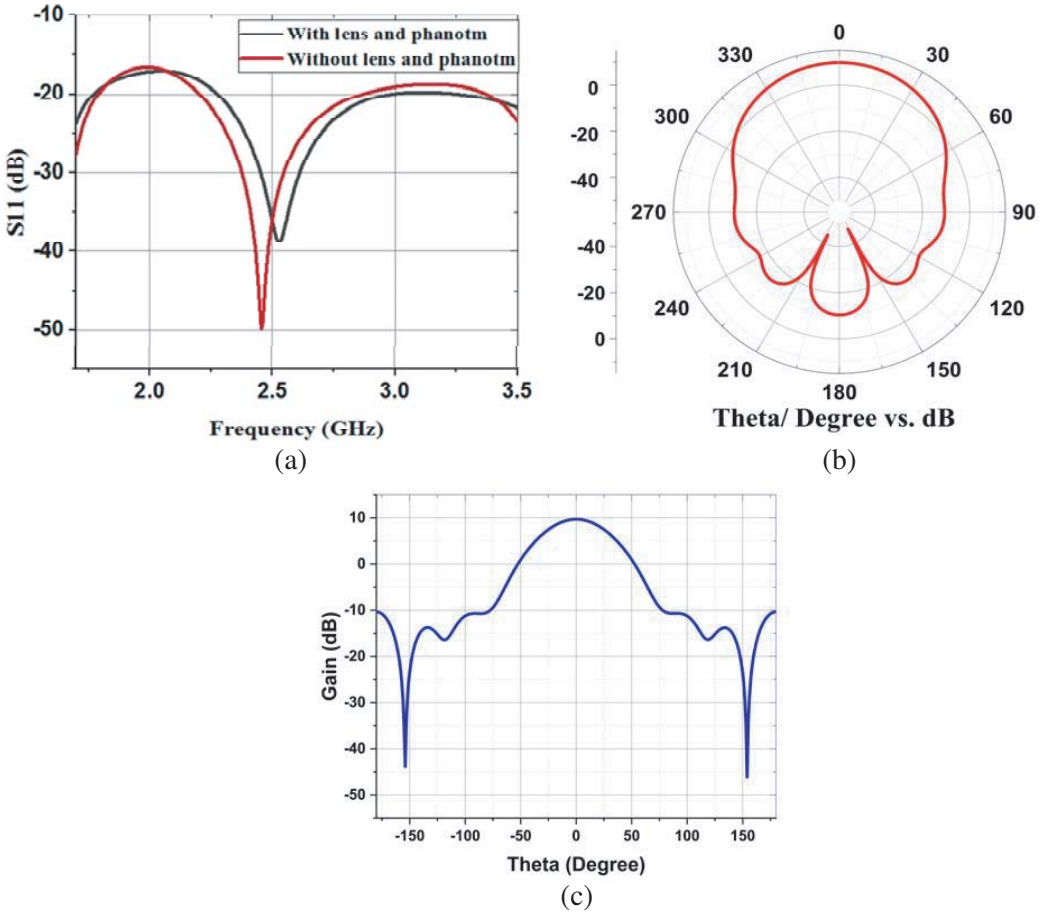

Figure 4. System radiator. (a) Reflection coefficient. (b) Radiation pattern (E-plane). (c) 2D E-plane radiation pattern.

2.3. Selecting Appropriate Matched Layer Permittivity

In the hyperthermia therapy system, the transmission coefficient of an electromagnetic wave at the phantom-air interface is directly proportional to the system efficiency either in breast imaging for

cancer detection or treatment [26]. From Eq. (6), the transmission coefficient would be affected by the total effective permittivity (ε_{eff}) of the breast phantom layers (skin, fat, glandular, and tumor). Hence, the transmission coefficient could be controlled through the total effective permittivity of the phantom layer aggregate. Adding another dielectric matched layer on the skin of the breast would change the transmission of the EM wave, which in turn would change the system power absorption. Effective permittivity in electromagnetic wave channelled through the human body is little different from a multipath channel because it includes multi-layers of tissues with different dielectric properties.

When an incident wave is normal to the interface of layers, which is the case in our study as shown in Fig. 5, effective permittivity is equal to the sum of a normalized weighted average function of the reciprocal of the permittivity values of the individual layers [27]. This case can be related to a parallel capacitor model represented by Eq. (7) [28].

$$\varepsilon_{eff} = \xi_1\varepsilon_1 + \xi_2\varepsilon_2 + \xi_3\varepsilon_3 + \xi_4\varepsilon_4 + \xi_5\varepsilon_5 \tag{7}$$

where ε_{eff}, $\varepsilon_{1\ldots5}$, and $\xi_{1\ldots5}$ are the total effective permittivity of the breast phantom layers, the permittivity of the phantom layers (skin, fat, glandular, tumor and matched layer), and the volume fraction of the constituent layers, respectively.

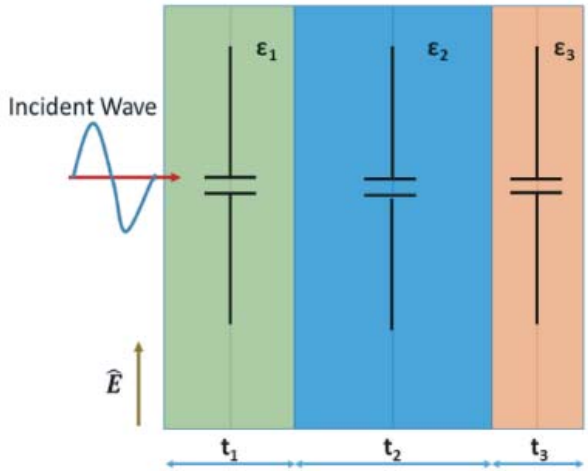

Figure 5. Parallel capacitive model for effective permittivity in the direction of the electric field.

The proposed thermal therapy system was applied to the scattered fibro glandular breast tissue of 25–50% glandular density [8]. Considering a matched layer with a thickness ($t = 1$ cm), the transmission coefficient of the EM wave at the air-phantom interface could be calculated in relation to the matched layer permittivity using Eqs. (6) and (7) as illustrated in Fig. 6. The matched layer permittivity was calculated for the tumor size in cancer stages I & II. In cancer stage I, tumor size is reported by American Joint Committee on Cancer (AJCC) to be between 0.4 and 2 cm, while in stage II, it is from 2 to 5 cm [29]. The permittivity and volumetric values of scattered breast layers used in calculations are represented in Fig. 1.

As represented in Fig. 6, the wave's transmission coefficient reached a maximum at specific values of matched layer permittivity. The tumor size did not have a significant effect on choice of the matched layer because the tumor was still in its early stage and deemed not to have spread in the phantom. This relation was verified by EM simulation when the proposed system was tested with and without the matched layer to examine its effect. Different thicknesses of dielectric matched layer ($t = 0.5$ & 1.5 cm) and their effect on transmission coefficient have been studied for more clarification as presented in Fig. 7.

A comparison between the calculated effective permittivity of phantom tissues with dielectric matched layer at thickness ($t = 1$ cm) and the real value of breast phantom in terms of transmission coefficient is developed as shown in Fig. 8. In scattered fibro glandular phantom, glandular tissue density is within 25%–50% [8] which produces a shift in reflection coefficient from calculated case.

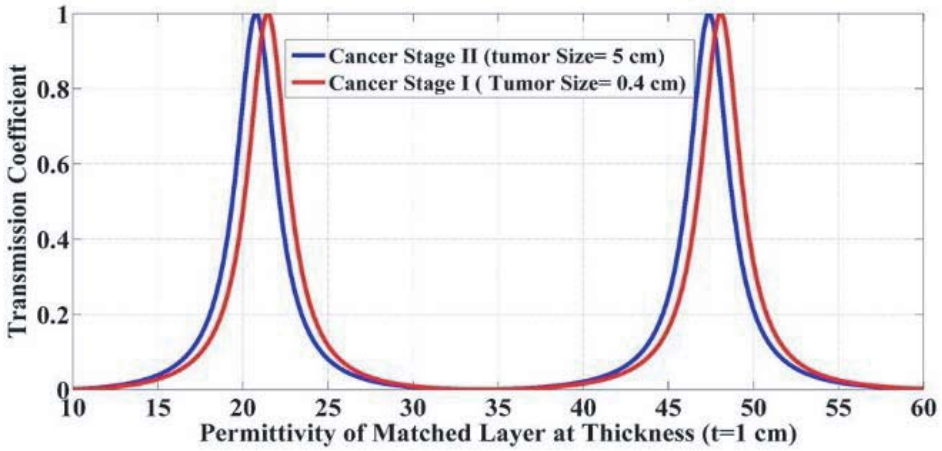

Figure 6. Transmission coefficient at the breast phantom-air interface with different matched layer permittivity at a thickness ($t = 1\,\text{cm}$).

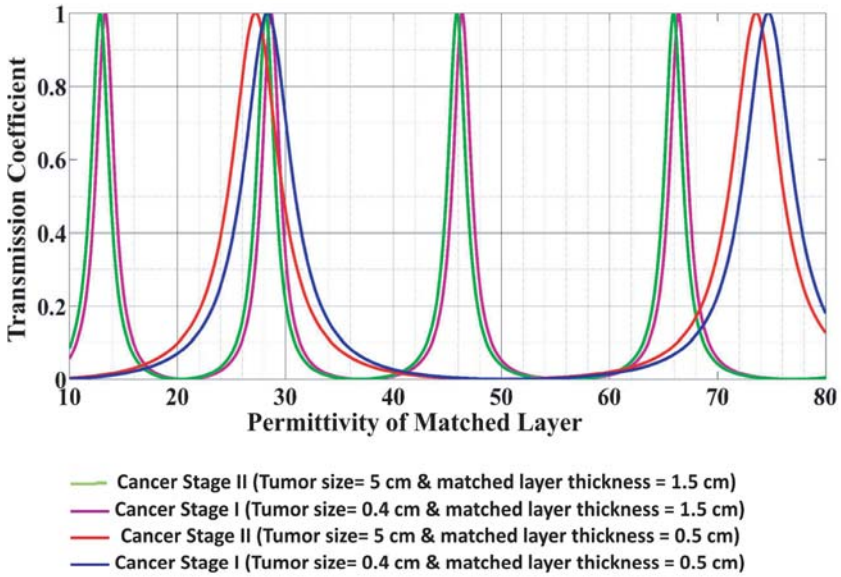

Figure 7. Transmission coefficient at the breast phantom-air interface with different matched layer permittivity and thickness ($t = 0.5$ & $1.5\,\text{cm}$).

3. SIMULATED SYSTEM SCENARIOS

Enhancing efficiency of the breast cancer hyperthermia therapy system was achieved in two steps. Firstly, the wave from the applicator to the breast phantom was increased by focusing with a convex lens. The proposed system consisted of a power source (horn antenna at 2.45 GHz) directed at the diseased phantom through the convex lens using 10.85 dBW of power for 2 minutes. Stage I breast cancer was represented by a spherical tumor ($R = 0.4\,\text{cm}$) at a depth of 1.5 cm from the breast skin. The proposed system is tested using multi-physics Computer Simulation Technology (CST) Microwave Studio simulator.

By adjusting the focal length of a convex lens placed 41.5 mm away using the same design concept discussed in [1] as shown in Fig. 1(a), EM power arriving at the tumor region was concentrated, resulting in an increase in temperature in the region from 35°C to 40°C as shown in Fig. 9(a) and Fig. 10(a). The

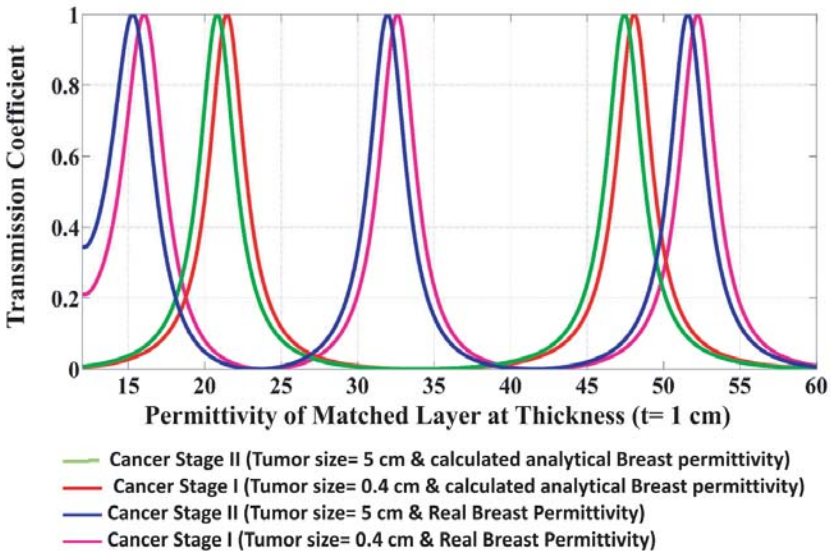

Figure 8. A comparison between real and calculated analytical breast permittivity at dielectric matched layer with thickness ($t = 1\,\text{cm}$).

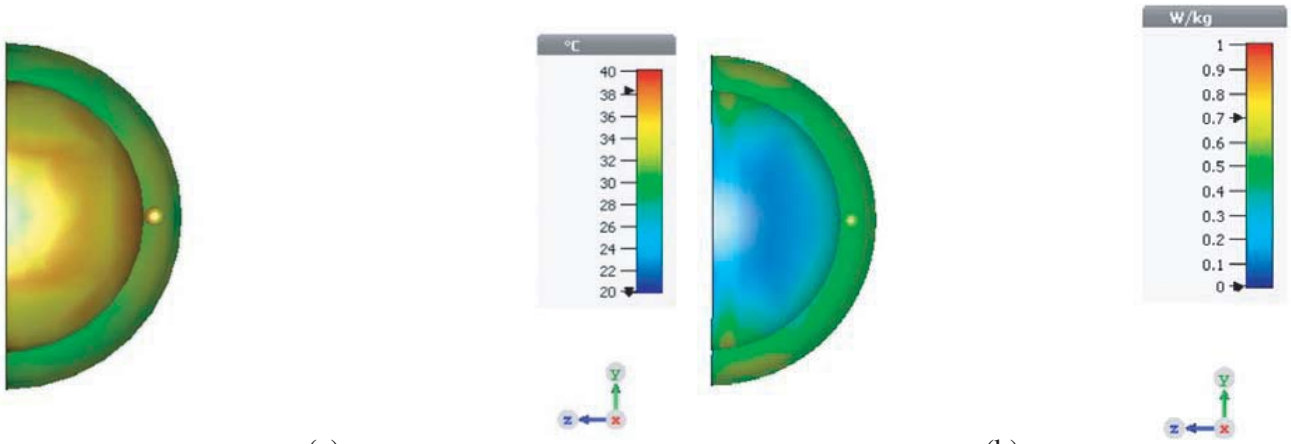

Figure 9. Diseased breast phantom without matched layer and convex lens. (a) Thermal. (b) SAR.

specific absorption rate (SAR) of the emitted power that was concentrated by the lens did not exceed the safety limit recommended by Federal Communications Commission (FCC) of the US Government (4.0 W/kg averaged over 10 grams of tissue), Fig. 9(b) and Fig. 10(b) [30].

Secondly, the system efficiency was enhanced by increasing the wave transmission to the breast layers. From Fig. 6, it can be seen that transmission was maximum at specific values, for example, ($\varepsilon = 21$) which was adopted for the EM simulation. Thermal and SAR readings in the tumor region were increased to almost 45°C and 3.3 W/kg, respectively, Figs. 11(a) and (b).

Adding a cooling layer is essential in a hyperthermia therapy system. In the proposed system, a water layer of 1.3 cm thickness was added on the dielectric matched layer to decrease skin temperature and the absorbed power to 42°C and 2.9 W/kg, respectively as shown in Figs. 12(a) and (b). Cancer stages I & II with different tumor sizes and depths were simulated for the situation after adding the dielectric matched layer and cooling layer as shown in Table 2.

Versatility of the proposed system could be increased by adding a second lens to help in heating more than one diseased region separately with only one wave source. Two spherical tumors of the same

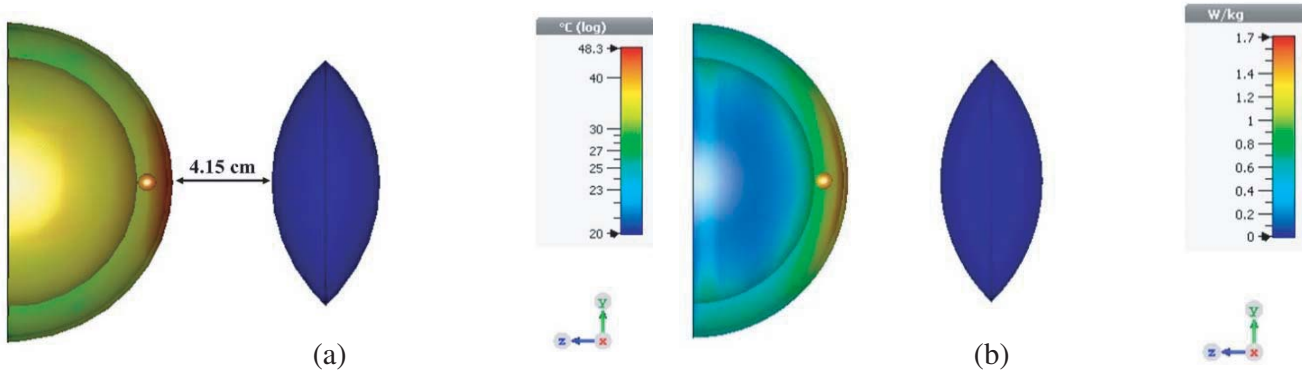

Figure 10. Diseased breast phantom with a convex lens. (a) Thermal. (b) SAR.

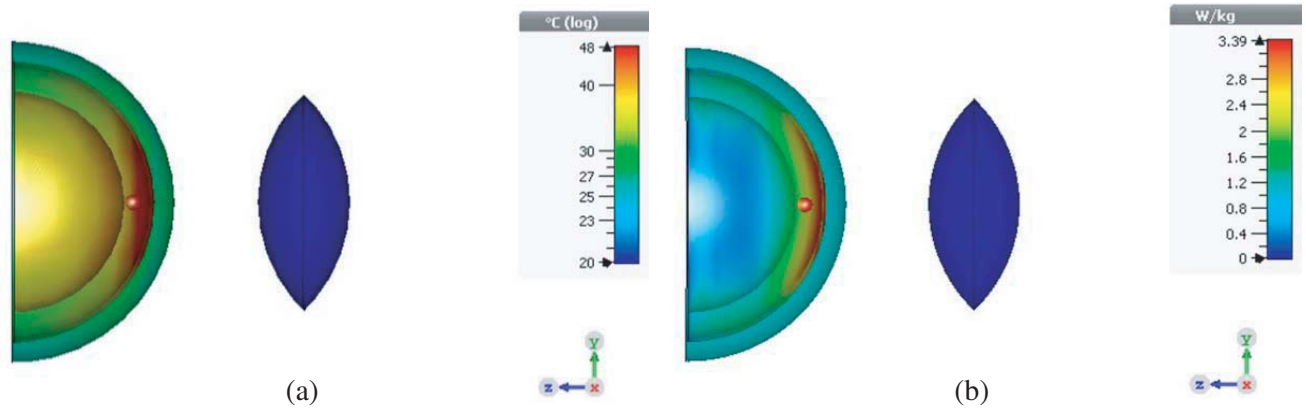

Figure 11. Diseased breast phantom with convex lens and dielectric matched layer ($t = 1\,\text{cm}$ and $\varepsilon = 21$). (a) Thermal. (b) SAR.

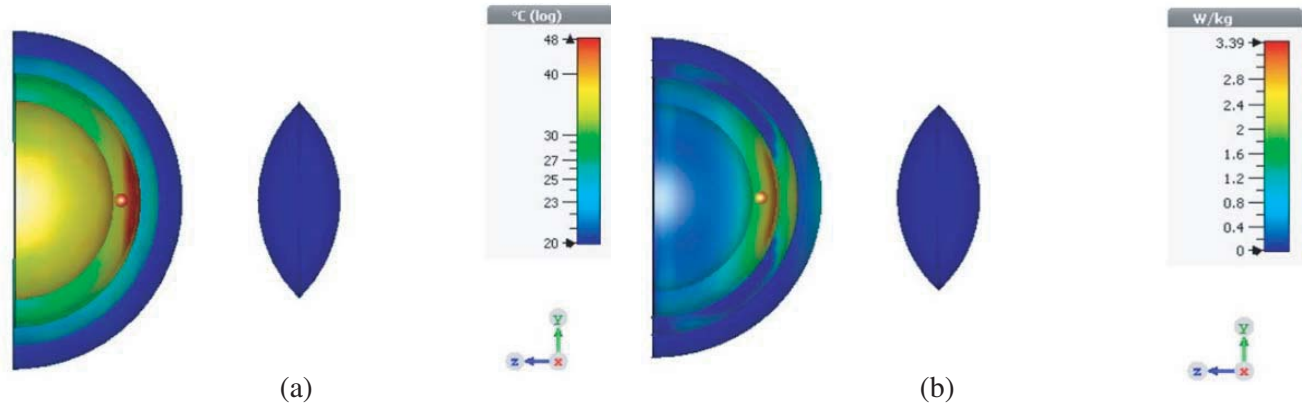

Figure 12. Diseased breast phantom with dielectric matched layer and cooling water. (a) Thermal. (b) SAR.

size ($R = 0.4\,\text{cm}$) were inserted in different regions under skin layer at a depth of 1.1 cm. Changing the inclination angles of each lens could increase tumor region temperature located at different locations in phantom.

Figure 13 depicts the effect of using two lenses with inclination angle ($\theta = 10°$) on SAR and the thermal distribution on two tumors regions. A comparison between system performances at different tumors locations using various inclination angles is shown in Table 3.

Table 2. Comparison of temperature and SAR attained for different tumor sizes and depths.

Tumor Radius R (cm)	Tumor Depth D (cm)	Cancer Stage	Temperature (°C)	SAR (W/kg)
1.5	2.2	II	48	3.4
0.5	1	I	47	3.3
1	1.7	I	45	3.2
2	2.7	II	41	1.2

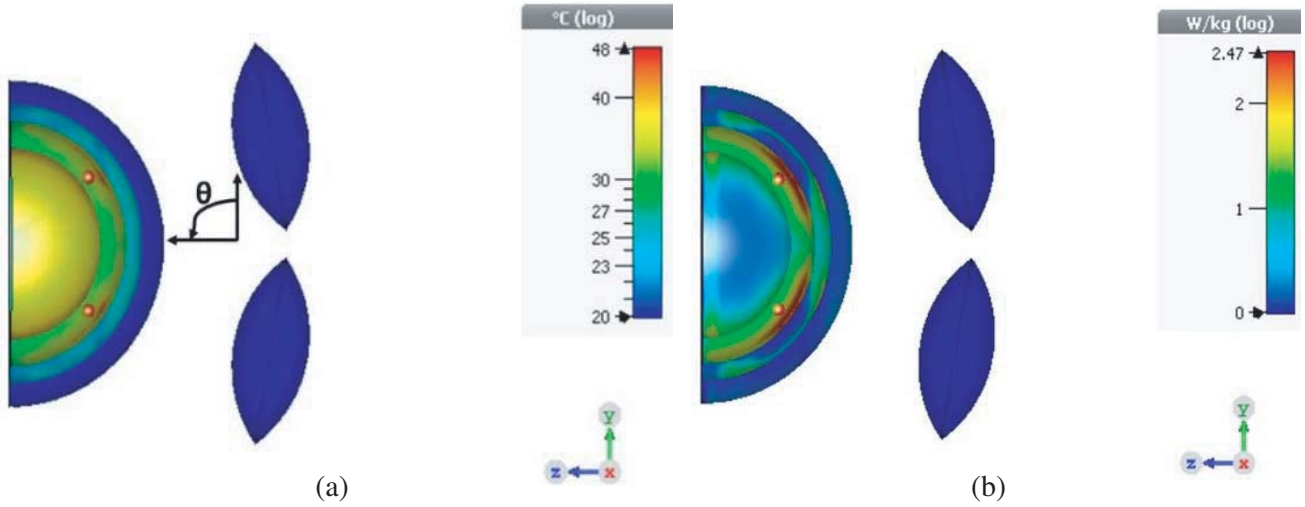

Figure 13. Diseased breast phantom with two convex lenses, dielectric matched layer and cooling water. (a) Thermal. (b) SAR.

Table 3. Comparison between performances of system with different lens inclination angles.

Inclination Angle (Degrees)		0°	10°	−10°
Tumor Location	y-axis (mm)	40.4	38	42
	z-axis (mm)	551	550	556
Temperature (°C)		44.5	45	45
SAR (W/kg)		2.2	2.3	2

4. FABRICATION AND MEASUREMENTS

To validate the analyzed and simulated system concept, the proposed hyperthermia therapy system was fabricated using available laboratory and fabrication facilities. Our study involved fabricating and measurements to validate the paper concept. As shown in Fig. 14, the prototype microwave hyperthermia system consisted of a power source (horn antenna at 2.45 GHz) that provided 10.85 dBW to the system, a container chamber of foam (Rohacell HF-71) which had a dielectric constant similar to air, a convex lens to focus power from the applicator to the tumor region, and a hemisphere foam container filled with an aqueous sugar-in-gelatin mixture that had the same effective permittivity of scattered-fibro glandular tissue.

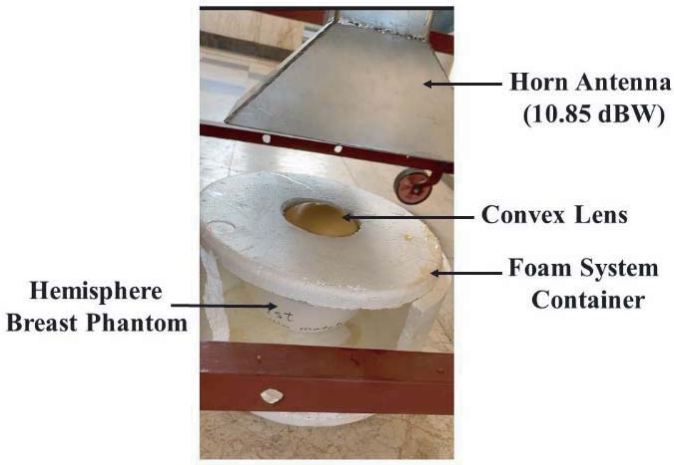

Figure 14. Proposed microwave thermal therapy system prototype.

4.1. Emulsion Matched Layer and Gelatin Phantoms

The developed tissue-mimicking (TM) materials were based on a sugar-in-gelatin mixture. Different proportions of gelatin and sugar were used to emulate the dielectric properties of breast tissue, dielectric matched layer, and tumor. The process of creating the required TM materials involved the following main steps. Firstly, based on the dielectric properties of water, sugar, and gelatin, mixtures of different ratios of those materials were used to achieve the required tissues dielectric properties. Secondly, the dielectric properties of the mixtures were measured. Third, the mixture ratios, especially for the gelatin, were adjusted to match the breast tissue dielectric properties.

The dielectric properties of the prepared samples were measured over the 2–4 GHz band using the Dielectric Assessment Kit Speag (DAK-3.5-TL2) with Vector Network Analyzer (VNA) Agilent 8719ES at room temperature as illustrated in Fig. 15(a). The measurement of the dielectric properties in DAK depends on open ended coaxial probe. The input reflection coefficient of the probe is measured with a network analyzer, and the permittivity is determined using an approximate circuit model for the probe admittance [31]. There are three main steps for measurement, including hardware installation, software installation, and calibration and measurements [32]. Many samples with different ratios are fabricated and measured through immersing DAK probe inside the sample and reading the result from PC as shown in Fig. 15(b). This process is repeated until reaching the required permittivity values. A side view of the fabricated breast phantom with tumor inside is presented in Fig. 15(c). The final compositions of the mixtures, as listed in Table 4, achieve the required permittivity of (43.7), (21), and (54) for breast, dielectric matched layer, and tumor, respectively at 2.45 GHz. These measured results matched the target values of the Debye model of breast tissues as discussed in Fig. 16 [33].

Table 4. Composition of breast phantom model at 2.45 GHz.

	Water	Gelatin	Sugar	Permittivity
Breast	70%	14.5%	14.5%	43.7
Matched Layer	50%	25%	25%	21
Tumor	85%	10%	5%	54

4.2. Convex Lens Fabrication

A 3D printer was used to fabricate the lens to the required dimensions as shown in Fig. 17. The fabrication process was performed with 100% infill at a resolution of 100 microns on PLA+ (Polylactic

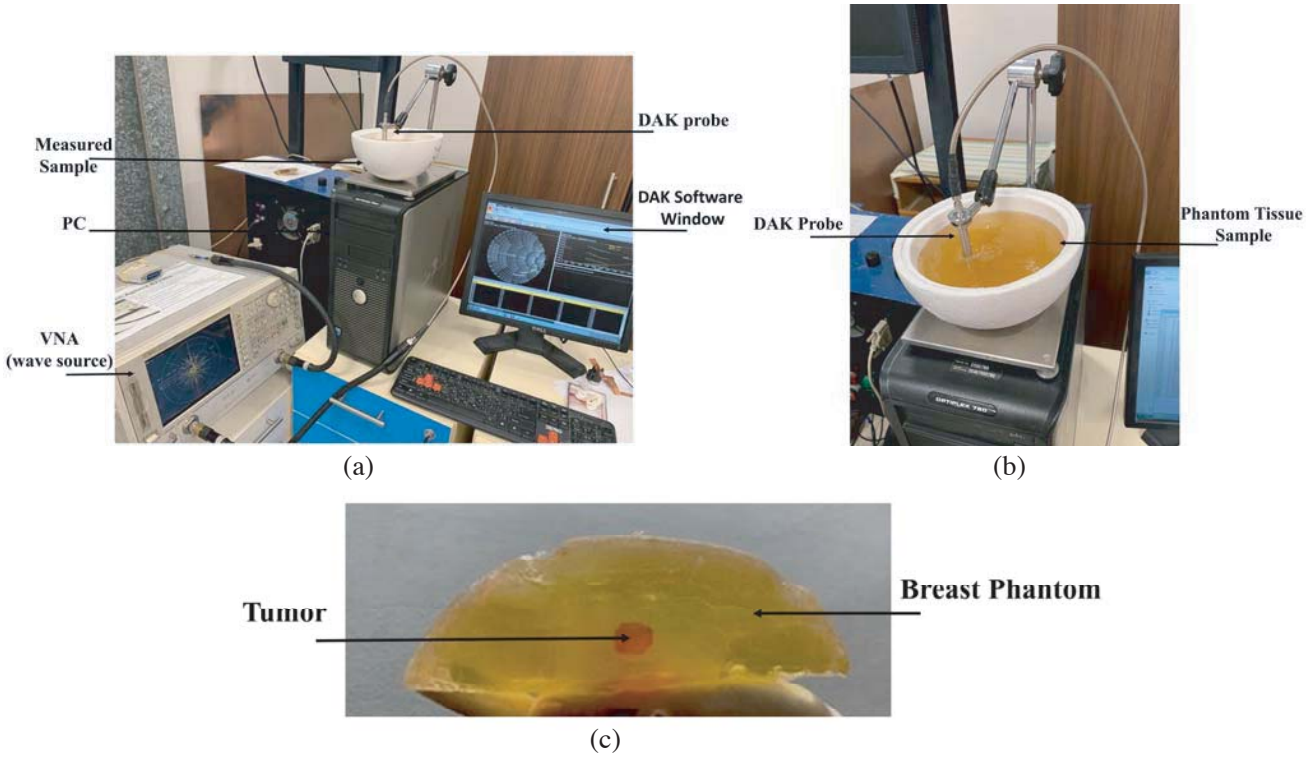

Figure 15. Gelatin tissues fabrications. (a) DAK hardware set up. (b) Measurement Process. (c) Fabricated diseased breast phantom.

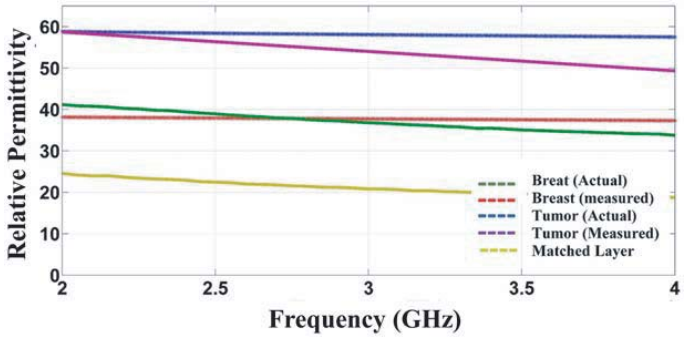

Figure 16. Comparison between measured and actual relative permittivity breast tissues.

acid) filament with the dielectric constant of $\varepsilon = 2.7$. The heat resistance of the PLA filament before deforming was around 85°C, which made it suitable for our application. The convex lens high temperature deformation resistance is important during hyperthermia therapy. The breast is exposed to high power for a period through convex lens which increases its temperature, so it should afford this temperature without deforming to do its mission properly.

4.3. Measurement Results

To validate the proposed system concept, the system components (applicator, a convex lens, and breast phantom) were arranged as shown in Fig. 14 to initiate measurement. The microwave power from the horn antenna (10.85 dBW) was focused on the diseased phantom through the convex lens for 2 minutes. The hyperthermia therapy system was tested in two cases: before heating and after heating (without

(a) (b)

Figure 17. Convex lens fabrication. (a) 3D printer process. (b) Final lens.

lens, with a lens, and with lens and dielectric matched layer). To confirm that focused heating occurred at the desired location, the tumor region temperature was measured before heating by manually placing the digital probe of the thermometers into the desired region. Tumor temperature ($R = 0.4$ cm and depth = 1.5 cm) of 19.6°C was regarded as the ambient temperature of the system. After heating the lens-free breast phantom for 2 minutes, the temperature of the tumor region rose to 23.9°C as shown in Fig. 18(a). The wave from the emitter was focused using a lens, as shown in Fig. 18(b), whereby the tumor region temperature increased further to 26.9°C. Adding a dielectric matched layer to the breast phantom greatly enhanced the temperature of the tumor region. As depicted in Fig. 18(c), the temperature reached 33.9°C in the lens-free case, a reading that was comparable to the simulated result.

With the application of both the convex lens and the dielectric matched layer in the complete proposed system, the temperature increased by 17.6°C from ambient to reach 37.2°C as shown in Fig. 18(d). The measured results approximated the simulation concept, which predicted an increase of 25°C. In the real case of diseased breast phantom, the normal ambient temperature of human

(a) (b) (c) (d)

Figure 18. Measured breast phantom. (a) Without dielectric matched layer and convex lens. (b) Without dielectric matched layer and with a lens. (c) With matched layer and without a lens. (d) With matched layer and lens.

Table 5. A comparison between previous hyperthermia systems and the proposed system.

	Proposed System	Ref. [15]	Ref. [34]	Ref. [35]
Operating Frequency (GHz)	2.45	2.45	1.8	0.915
Amplitude of used power	10.85 dBW	53.5 V/cm for each source element	1.5 dBW for each source element	6.8 dBW for each feeder
Exposure Time (min)	2	60	30	60
No. of power source elements	One horn antenna	4 flat LHM lens applicator	16 planar flexible antennas	4 feeder of ($\lambda/2$) dipole antenna with short stub
Treatment of two tumors simultaneously	yes	No	No	No
Increased Temperature (oC)	17.6	6	16	10

breast is almost 37°C, and by using the proposed system for hyperthermia treatment, the tumor region temperature will increase above 42°C which is the required temperature range for breast cancer treatment. For more clarification about the proposed system characteristics, a comparison with previous systems is summarized in Table 5.

5. CONCLUSION

A microwave hyperthermia therapy preclinical system was designed based on analytical calculations. The proposed system was tested on cancer stages I & II at different depths in the breast phantom. A horn antenna has been designed at an analytically chosen frequency (2.45 GHz) through studying EM wave transmission and reflection coefficients at the air-phantom interface. A dielectric matched layer technique has been added to breast skin layer to enhance the system efficiency without increasing the system applied input power. A cooling water layer was applied to ensure normal temperature at the patient skin. Simulated and experimental results have clarified that such a system can achieve suitable focusing and heating for the potential represented application of microwave breast cancer hyperthermia.

ACKNOWLEDGMENT

This work was supported by the Mission Department of the Ministry of Higher Education in Egypt and Egypt-Japan University of Science and Technology (E-JUST).

REFERENCES

1. Abdel-Haleem, M. R., T. Abouelnaga, S. M. Ahmed, et al., "Convex lenses horn antenna microwave hyperthermia scheme," *12th European Conference on Antennas and Propagation (EuCAP)*, London, UK, 2018.
2. Choi, W. C., S. Lim, and Y. J. Yoon, "Design of noninvasive hyperthermia system using transmit-array lens antenna configuration," *IEEE Antennas and Wireless Propag. Lett.*, Vol. 15, 857–860, 2015.

3. Nguyen, P. T., A. Abbosh, and S. Crozier, "Three-dimensional microwave hyperthermia for breast cancer treatment in a realistic environment using particle swarm optimization," *IEEE Trans. Biomed. Eng.*, Vol. 64, No. 6, 1335–1344, 2017.
4. Tao, Y. and G. Wang, "Conformal hyperthermia of superficial tumor with cylindrical left-handed metamaterial lens applicator," *Progress In Electromagnetics Research C*, Vol. 66, 1–10, 2016.
5. Tao, Y., E. Yang, and G. Wang, "Left-handed metamaterial lens applicator with built-in cooling feature for superficial tumor hyperthermia," *Appl. Computational Electromagnetics Society J.*, Vol. 32, No. 11, 1029–1034, 2017.
6. Asili, M., P. Chen, A. Z. Hood, et al., "Flexible microwave antenna applicator for chemo thermotherapy of the breast," *IEEE Antennas and Wireless Propag. Lett.*, Vol. 14, 1778–1781, 2014.
7. Datta, N. R., et al., "Local hyperthermia combined with radiotherapy and/or chemotherapy: Recent advances and promises for the future," *Cancer Treat. Reviews*, Vol. 41, No. 9, 742–753, 2015.
8. ACR, *ARC BI-RADS Atlas*, American College of Radiology, USA, 2013.
9. Giuliano, A. E., J. L. Connolly, S. B. Edge, et al., "Breast cancer-major changes in the American Joint Committee on Cancer eighth edition cancer staging manual," *A Cancer J. for Clinicians*, Vol. 67, No. 4, 290–303, 2017.
10. Nguyen, P. T., A. Abbosh, and S. Crozier, "Three-dimensional microwave hyperthermia for breast cancer treatment in a realistic environment using particle swarm optimization," *IEEE Trans. Biomed. Eng.*, Vol. 64, No. 6, 1335–1344, 2016.
11. Stang, J., M. Haynes, P. Carson, and M. Moghaddam, "A preclinical system prototype for focused microwave thermal therapy of the breast," *IEEE Trans. Biomed. Eng.*, Vol. 59, No. 9, 24131–2438, 2012.
12. He, X., W. Geyi, and Sh. Wang, "Optimal design of focused arrays for microwave-induced hyperthermia," *IET Microw., Antennas Propag.*, Vol. 9, No. 14, 1605–1611, 2015.
13. Curto, S., T. S. P. See, P. McEvoy, et al., "In-silico hyperthermia performance of a near-field patch antenna at various positions on a human body model," *IET Microw., Antennas Propag.*, Vol. 5, No. 12, 1408–1415, 2011.
14. Karnik, N. S. R. Tulpule, M. Shah, et al., "Design, simulation and experimental study of near-field beam forming techniques using conformal waveguide arrays," *IET Microw., Antennas Propag.*, Vol. 4, No. 2, 162–174, 2010.
15. Wang, G. and Y. Gong, "Metamaterial lens applicator for microwave hyperthermia of breast cancer," *Int. J. Hyperthermia*, Vol. 25, No. 6, 434–445, 2009.
16. Tao, Y. and G. Wang, "Conformal hyperthermia of superficial tumor with cylindrical left-handed metamaterial lens applicator," *Progress In Electromagnetics Research C*, Vol. 66, 1–10, 2016.
17. Keshavarz, S., A. Abdipour, A. Mohammadi, and R. Keshavarz, "Design and implementation of low loss and compact microstrip triplexer using CSRR loaded coupled lines," *International Journal of Electronics and Communications (AEÜ)*, Vol. 111, 2019.
18. Keshavarz, S. and N. Nozhat, "Dual-band Wilkinson power divider based on composite right/left-handed transmission lines," *13th International Conference on Electrical Engineering/Electronics, Computer, Telecommunications and Information Technology (ECTI-CON)*, Thailand, 2016.
19. Harrington, R. F., Spherical Wave Function, *Time-Harmonic Electromagnetic Fields*, McGraw-Hill, New York, NY, USA, 1961.
20. Luhn, S. and M. Hentschel, "Analytical Fresnel laws for curved dielectric interfaces," *Journal of Optics*, Vol. 22, 2020.
21. Lazebnik, M., D. Popovic, L. McCartney, et al., "A large-scale study of the ultrawideband microwave dielectric properties of normal, benign and malignant breast tissues obtained from cancer surgeries," *Physics in Medicine and Biology*, Vol. 52, No. 20, 6093–6115, 2007.

22. Ashok Kumar, S. and T. Shanmuganantham, "Design and analysis of implantable CPW fed bowtie antenna for ISM band applications," *AEU — Int. J. of Electron. and Commun.*, Vol. 68, No. 2, 158–165, 2014.
23. Ashok Kumar, S. and T. Shanmuganantham, "Design of implantable CPW fed monopole H-slot antenna for 2.45 GHz ISM band applications," *AEU — Int. J. of Electron. and Commun.*, Vol. 68, No. 7, 661–666, 2014.
24. Ivashina, M. V., J. Simons, and J. G. Bij De Vaate, "Efficiency analysis of focal plane arrays in deep dishes," *The Square Kilometre Array: An Engineering Perspective*, 149–162, Dordrecht, Springer, 2005.
25. Dahri, M. H., M. H. Jamaluddin, F. C. Seman, et al., "Aspects of efficiency enhancement in reflectarrays with analytical investigation and accurate measurement," *Electronics*, Vol. 9, No. 11, 2020.
26. Gholipur, T. and M. Nakhkash, "Optimized matching liquid with wide-slot antenna for microwave breast imaging," *AEU — Int. J. of Electron. and Commun.*, Vol. 85, 192–197, 2018.
27. Pe'rez Cesaretti, M. D., "General effective medium model for the complex permittivity extraction with an open-ended coaxial probe in presence of a multilayer material under test," Ph.D. dissertation, University of Bologna, Italy, 2012.
28. Hu, F., J. Song, and T. Kamgaing, "Modeling of multilayered media using effective medium theory," *19th Conference on Electrical Performance of Electronic Packaging and Systems*, USA, Oct. 2010.
29. Gabriel, N. H., L. C. James, J. D. Carl, et al., "AJCC cancer staging manual," *American Joint Committee on Cancer (AJCC)*, 589–628, Springer, New York, 2017.
30. Council of the European Union, "Council Recommendation: On the limitation of exposure of the general public to electromagnetic fields (0 Hz to 300 GHz)," *Official Journal of the European Communities*, 1999.
31. Meaney, P., T. Rydholm, and H. Brisby, "A transmission-based dielectric property probe for clinical applications," *Sensors*, Vol. 18, No. 10, 3484, 2018.
32. SPEAG, *DAK Professional Handbook V2.4*, Schmid & Partner Engineering AG, Switzerland, 2016.
33. Lazebnik, M. and M. Okoniewski, "Highly accurate debye models for normal and malignant breast tissue dielectric properties at microwave frequencies," *IEEE Microw. Wireless Compon. Lett.*, Vol. 17, No. 12, 822–824, 2007.
34. Dadzadi, A. and R. Faraji-Dana, "Breast cancer hemispheric shaped hyperthermia system designed with compact conformal planar antenna array," *IEEE Asia-Pacific Microwave Conference (APMC)*, Singapore, 2019.
35. Choi, W. C., S. Lim, and Y. J. Yoon, "Evaluation of transmit-array lens antenna for deep-seated hyperthermia tumor treatment," *IEEE Antennas and Wireless Propagation Letters*, Vol. 19, No. 5, 866–870, 2020.